DOI 10.1007/s11148-018-0238-9
Refractories and Industrial Ceramics *Vol. 59, No. 4, November, 2018*

MICROSTRUCTURE AND PROPERTIES OF THE MULLITE–$ZrO_2(Y_2O_3)$–Si_3N_4-COMPOSITE CERAMICS SINTERED IN BY DIFFERENT METHODS

G. Sedmale,[1,3] L. Grase,[1] I. Zalite,[1] N. Zilinska, and J. Rodrigues[2]

Translated from *Novye Ogneupory*, No. 7, pp. 49 – 54, July 2018.

Original article submitted February 13, 2018.

The purpose of the study was to investigate densification, phase composition, microstructure and properties of mullite–ZrO_2 composite ceramics with the Si_3N_4 additive, sintered by various methods: conventional sintering, spark-plasma sintering, and sintering in both microwave and solar furnaces. The strength properties (compressive strength and elastic modulus) of the ceramic samples sintered by the conventional method and by spark-plasma sintering were compared. Some reasons for the formation of defects in the samples after sintering in microwave and solar furnaces are indicated

Keywords: mullite–$ZrO_2(Y_2O_3)$–Si_3N_4 composite ceramics, Si_3N_4 nanopowder, spark-plasma sintering (SPS), microwave furnace (MW), solar furnace (SF).

INTRODUCTION

It is known [1] that mullite ceramics are widely used in high-temperature processes, wherein preservation of high thermomechanical properties is critical. A number of specific properties of such ceramics — resistance to temperature changes and aggressive chemical media, in some cases electrical characteristics — are often improved by modifying the composition of the ceramics by adding ZrO_2 (or $ZrSiO_4$), magnesium oxide, lanthanum [2, 3]. Very important in the synthesis of mullite ceramics is the sintering process, which can be accelerated, for example, when kaolinite is used as the raw material, by its thermal decomposition followed by interaction with Al_2O_3 [4]. In recent years, to intensify the process of mullite formation, alternative methods of sintering have been used, which shorten synthesis duration while simultaneously densifying the initial powder and ensuring the formation of the mullite crystalline phase. In these cases, the ceramic material is synthesized by hot pressing, sintering in a microwave (MW) or solar furnace (SF), or by spark plasma sintering (SPS).

In the case of microwave sintering [5 – 7], heat is transferred in the bulk of the material by electromagnetic waves. Moreover, a higher densification and better stabilization of the tetragonal ZrO_2 phase is achieved in the mullite-ZrO_2 composites than with conventional sintering. In turn, in a solar furnace, the necessary temperature is reached in a very short time [8, 9]. Despite the high cost of solar furnaces, some positive aspects of using this type of sintering are notable: solar energy is a renewable resource, and the purchase of very costly solar furnaces on average quickly pays off. Therefore, this method provides better densified ceramic materials with a characteristic microstructure and thus makes it possible to vary their properties.

The purpose of this work is to study the sintering process that affects the formation of the microstructure, the composition of the crystalline phase, and certain properties of mullite–$ZrO_2(Y_2O_3)$–Si_3N_4 ceramics sintered by SPS or in a MW and SF. Obtained data were compared with similar parameters of ceramic samples sintered by the conventional method.

RESEARCH METHODS

The initial mixture of the mullite–$ZrO_2(Y_2O_3)$–Si_3N_4 composition was prepared from chemically pure (>99% pure) oxides γ-Al_2O_3, monoclinic ZrO_2, Y_2O_3 (purchased

[1] Riga Technical University, Institute of Silicate Materials, Riga, Latvia.
[2] Platforma Solarde Almeria, Tabernas, Spain.
[3] gaida-maruta.sedmale@rtu.lv

TABLE 1. Composition of the Initial Composite Mixture, wt. %

Designation of the composition	γ-Al_2O_3	Quartz sand (SiO_2 98.7%)	ZrO_2 mon	Y_2O_3	Si_3N_4
MN0	62.30 – 59.20	28.42 – 27.05	5.20 – 4.90	4.50 – 4.2	0
MN1				5	1
MN5					5

from Nabaltec) and Si_3N_4 (~1:1 α- and β-forms); SiO_2 was introduced in the form of purified quartz sand (SiO_2 98.7%, Al_2O_3 1.3%). The composition of the initial mixture is given in Table 1. The resulting mixture was homogenized and ground in a Retsch PM-100 planetary ball mill for 10 hrs in an ethyl alcohol medium, and dispersity was then determined by the nitrogen adsorption (BET) method using a Nova 1200e analyzer. The specific surface area of the powder without additives and with the addition of 5% Si_3N_4 was 27.85 and 52.50 m^2/g, respectively; with the addition of Si_3N_4 nanopowder it was 85.25 m^2/g. Behavior of the powder upon heating to 1500°C was analyzed by differential thermal analysis (DTA) using a Setaram, Setsys Evolution 1750 instrument in helium atmosphere. The Atlas Power Hydraulic Press was used to pellet the powder into samples in the form of cylinders 30 – 35 in tall and 30 mm in diameter to determine the compressive strength, and in the form of rods 50 mm long with a cross-sectional area of 14 – 16 mm^2 to determine the elastic modulus and heat resistance. Thus, the samples in the form of cylinders and rods were made for conventional and microwave sintering. For sintering in a solar furnace, only disks about 25 mm diameter with a thickness of about 2.5 mm were made. Samples for SPS were formed from the powder directly in the furnace.

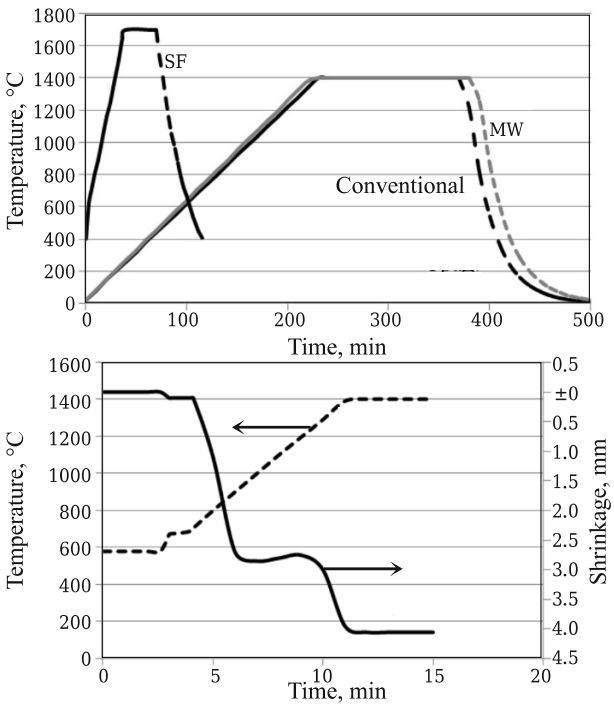

Fig. 1. Heating curves of samples during sintering in a SF, MW, by the conventional method (*a*) and by SPS (*b*).

Reactive synthesis (sintering) by the conventional method was carried out in a Nabertherm-3000 furnace in nitrogen atmosphere at a maximum temperature of 1400°C with a heating rate of 6°C/min and 2 hr isothermal hold. SPS was performed using a Sumitomo SPS-825.CE (Dr. Sinter, Japan) machine at a maximum temperature of 1400°C. In this case, the samples were formed in graphite molds at a pressure of 3 kg/cm^2 under vacuum in the range of 500 – 1400°C. Vacuum was kept constant at about 6 Pa. Microwave sintering was carried out in a laboratory furnace MHTD-1800 – 2.45/4.82 with a heating rate of 7°C/min and isothermal holding time of 2 hr. Sintering in a solar furnace, however, was not strictly controlled. In the selected solar furnace SF 40, designed in Spain (Platforma Solarde Almeria), the solar flux is concentrated only in a small area. Therefore, before the entire sample reached the maximum and uniform temperature, apparently, stresses formed in the samples that caused fracture or even destruction of the samples during cooling. The heating curves of the samples prepared by various sintering methods are shown in Fig. 1.

The degree of sintering (densification, %) was estimated from the change in the relative density according to the ratio d_1/d_0 from the density data determined according to Archimedes' principle; the density of the sintered ceramic sample was compared with the theoretically possible calculated density (3.35 g/cm^3) of the investigated composition. The density and complete shrinkage of the sintered samples were determined according to EN LVS 63-01:2001. Compressive strength of three samples was measured simultaneously according to LVS EN 14617 using a Toni Technic model 2020 instrument. Heat resistance was determined according to ASTM C1525 from the change in the elastic modulus during thermal cycling of the sample (1000°C – water) taking into account ASTM E1876-01 using a Buzz-o-Sonic device (BuzzMac International, USA) with subsequent calculations [10]. Microstructure and phase composition were analyzed using a Nova NanoSEM model 650 (the Netherlands) scanning electron microscope (SEM) and a D8 Advance (Bruker) diffractometer with Cu K_α-radiation, scan interval $2\theta = 10 – 60$ degrees at a scan speed of 4 deg/min.

RESULTS AND DISCUSSION

Characteristics and behavior of the starting powder in traditional sintering

After homogenization and grinding, the initial powder mixture was in the form of agglomerates formed from weakly bonded particles (Fig. 2). With the addition of Si_3N_4 nanopowder, agglomeration was apparently intensified and the resulting agglomerates had a more obvious interface.

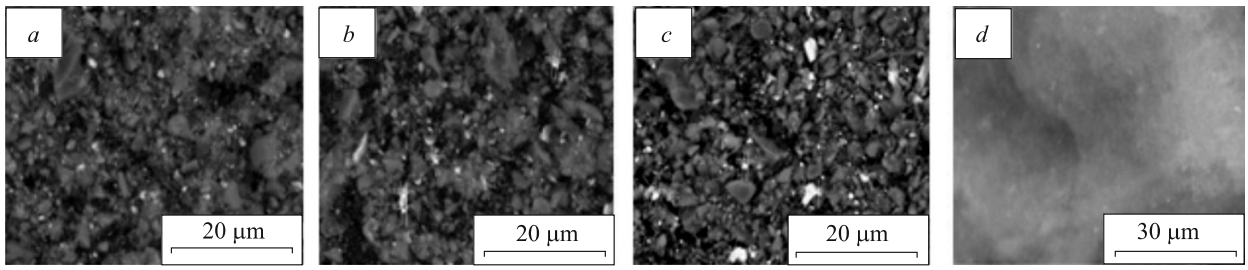

Fig. 2. SEM images of the original powder without the addition of Si_3N_4 nanopowder (*a*), with the addition of nanopowder in the amount of 1 (*b*) and 5% (*c*); *d*) SEM image of Si_3N_4 nanopowder.

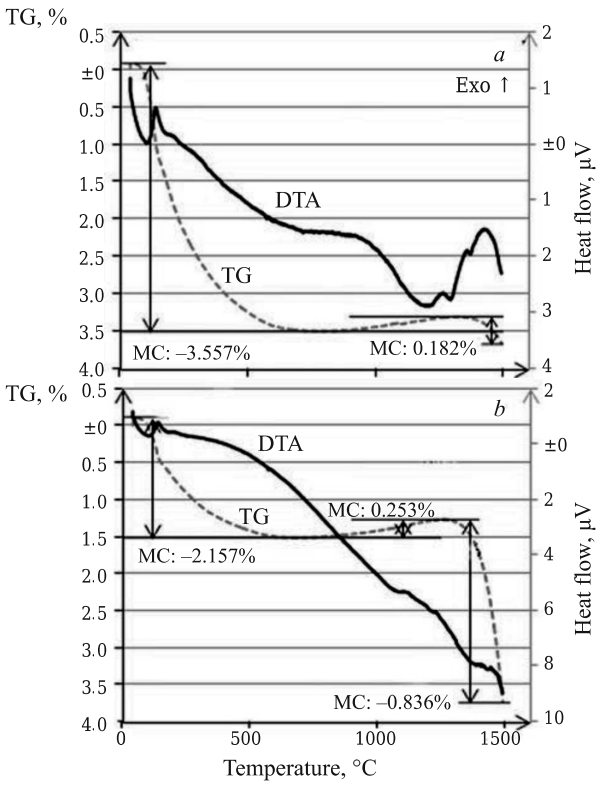

Fig. 3. *DTA* and *TG* curves of the initial powders without additives (*a*) and with the addition of 5% Si_3N_4 (*b*).

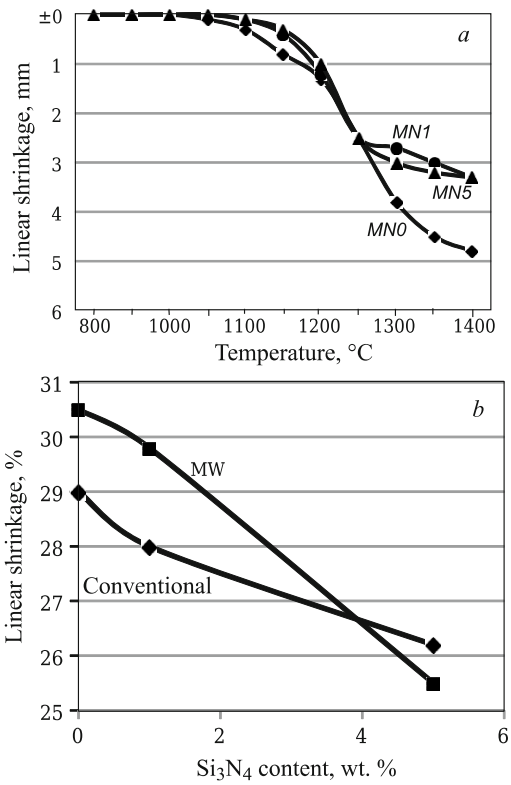

Fig. 4. Linear shrinkage of ceramic samples produced by SPS (*a*), sintering in a MW and the conventional method (*b*).

Light-colored separate points outside the agglomerates in all likelihood were ZrO_2 (see Fig. 2).

The shape of the *DTA* and *TG* curves (Fig. 3) shows that the main processes during heating with the traditional sintering method are the decomposition and transformation of the original components to a temperature of about 1200°C, at which a certain amount of the liquid phase accompanying the onset of crystallization is formed. A clearly expressed endothermic effect at initial heating temperatures below 200°C is due to the release of hygroscopic moisture from the surface of the powder particles. An unclear exothermic effect in the 900 – 950°C range is apparently due to the onset of crystallization of mullite. As can be seen, the shape of *DTA* curves of the original powder with and without the addition of 5% Si_3N_4 is similar. The difference is that the addition of 5% Si_3N_4 leads to an increase in the crystallization temperature and a change in the shape of the *TG* curve, mainly due to the decomposition of Si_3N_4.

Densification of samples during sintering

The sintering process, accompanied by shrinkage and densification of samples in different gas media under various temporal-temperature conditions in the furnace, varies. Fig. 4 shows the change in linear shrinkage of samples obtained by SPS and sintering in a MW in comparison with the conventional method. Shrinkage of the samples produced in a SF could not be determined due to sample fracturing. Sintering in a MW and by the conventional method is accompanied by

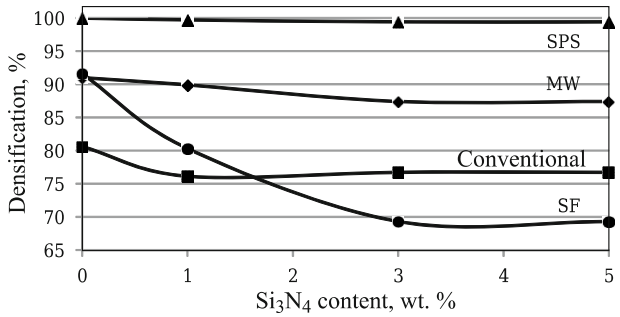

Fig. 5. Densification of ceramic samples at 1400°C, sintered by the conventional method, SPS, in a MW and a SF.

a very significant shrinkage with a tendency to decrease in samples with the addition of Si_3N_4. At the same time, densification of samples changes little with the addition of Si_3N_4, except for samples sintered in a SF (Fig. 5). In all likelihood, rapid increase and uneven distribution of temperature throughout the sample volume in the case of sintering in a SF leads not only to the appearance of fractures, but also to the formation of closed pores. Maximized sintering is achieved by the SPS method. This method, simultaneously ensuring the effect of high temperature under vacuum and pressure on the powder sample, greatly accelerates particle diffusion and thereby the processes of sintering and densification, maximally eliminating the formation of any defects.

Mechanical and thermal properties

Mechanical properties change according to the same pattern. Fig. 6 shows the change in the elastic modulus of ceramic samples obtained by SPS and conventional sintering, depending on the content of the Si_3N_4 additive. According to the standard [11], these data actually show a change not only in the elastic modulus, but also in the resistance of the material to sudden thermal changes. As can be seen from Fig. 6, the values of *E* differ not only in ceramic samples not subjected to thermal shock, but also after the first thermal cycle, decreasing by almost 50%, as in the samples with the addition of Si_3N_4 obtained by SPS and the conventional method. However, in ceramic samples obtained by SPS, with the increase in the number of thermal shock cycles, especially in samples without additives, the values of *E* do not decrease by more than 30%, which makes it possible to classify these ceramic samples as heat-resistant. It should be noted that the decrease in the elastic modulus after the first thermal shock cycle and its subsequent increase in samples obtained by SPS arise because of the formation of internal defects in them, most probably microfractures self-healing after the second or third cycle when a certain amount of liquid phase appears due to heating. In conventionally sintered samples, the rapid decrease in the elastic modulus already after the first thermal cycle is due, apparently, to the presence of closed pores that formed during sintering as a result of decomposition of Si_3N_4.

These results and the summarized densification values of the sintered samples are correlated with compressive strength data (Table 2), that are relatively high both in the samples obtained by SPS and by sintering in a MW, but are much lower for the samples sintered by the conventional method.

Phase composition and microstructure

In the sintering process, the dominant crystalline phase is mullite with an average crystal size of 50 – 80 nm. X-ray diffraction spectra of samples prepared by all the used sintering methods are similar. Therefore, x-ray diffraction spectra of only the samples obtained by the conventional sintering method and by SPS are shown in Fig. 7. The main differences are in the resulting crystalline modification of ZrO_2. In

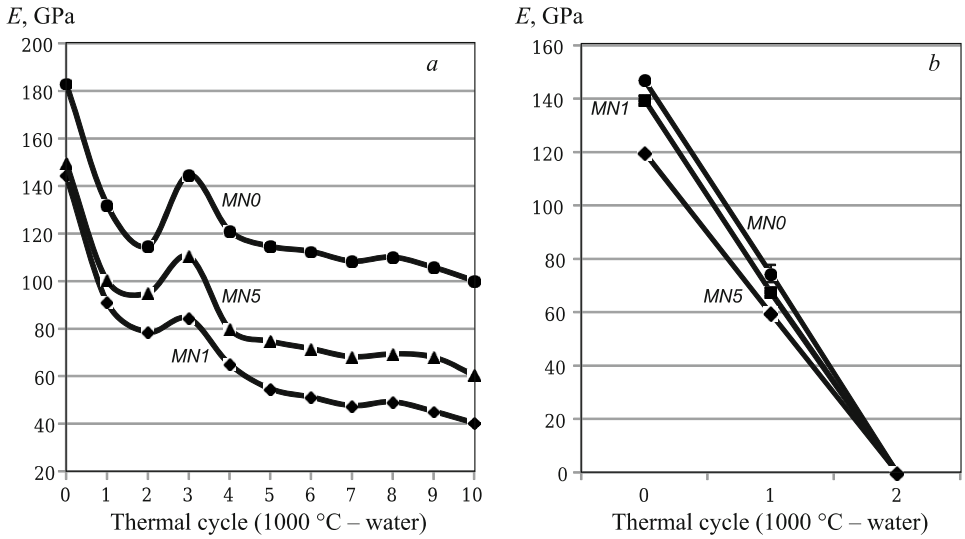

Fig. 6. Changes in the elastic modulus *E* of ceramic samples obtained by SPS (*a*) and conventional sintering (*b*), as a function of the number of thermal shock cycles.

TABLE 2. Compressive Strength of Ceramic Samples Obtained by Conventional Sintering, SPS and in a MW

Composition (see Table 1)	Compressive strength, MPa, depending on the sintering method		
	Conventional	SPS	MW
MN0	195	460	405
MN1	160	475	401
MN5	98	598	395

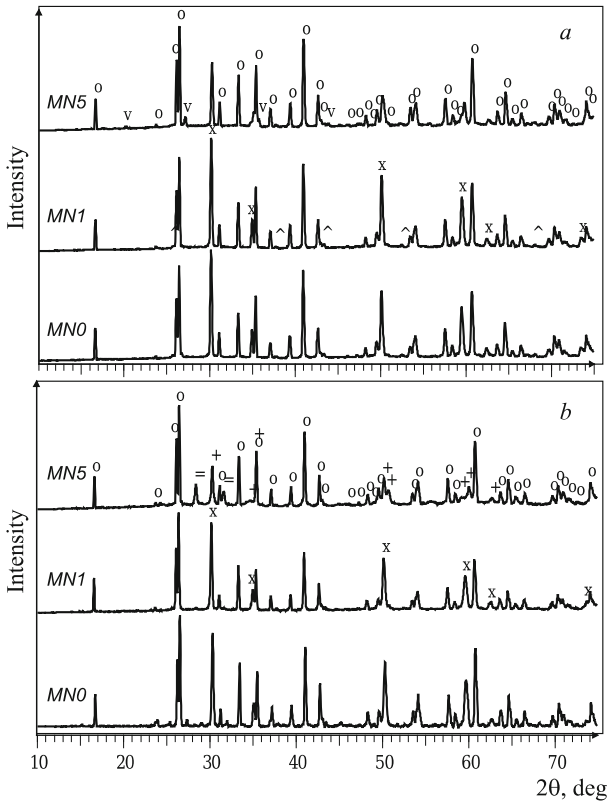

Fig. 7. X-ray diffraction spectra of samples obtained at 1400°C by conventional sintering (*a*) and SPS (*b*): ○) mullite; ×) cubic ZrO_2; V) zircon sand; ^) corundum; +) tetragonal ZrO_2; =) monoclinic ZrO_2.

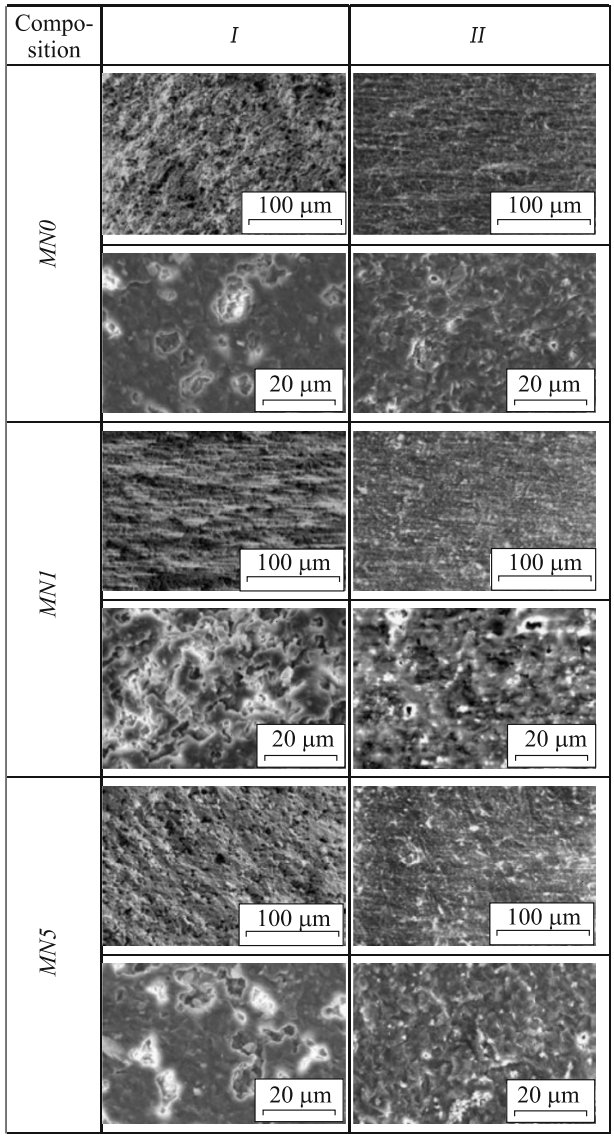

Fig. 8. SEM micrographs of ceramic samples of different compositions (see Table 2) obtained at 1400°C by traditional sintering (*I*) and SPS (*II*).

the samples sintered by SPS (see Fig. 7*b*), three main phases of zirconium oxide are formed: tetragonal ZrO_2, cubic ZrO_2, and monoclinic ZrO_2 impurities, the crystallization intensity of which, according to the intensity of the compared reflections, varies depending on the content of the additive Si_3N_4. At the same time, in the samples prepared by conventional sintering, cubic ZrO_2 is predominant along with zircon sand $ZrSiO_4$ and corundum α-Al_2O_3 impurities.

SEM micrographs of ceramic samples sintered using all the aforementioned types of sintering are characterized by the presence of closely packed characteristic prismatic formations of mullite. However, ceramics obtained by traditional sintering, and especially by SPS (Fig. 8), exhibit some deviation from prismatic forms characteristic for mullite and the presence of "voids" (or closed pores) in which secondary crystalline formations of mullite can be observed. In general, the microstructure of SPS-samples is denser, however, rarefied fine pores are formed with the addition of Si_3N_4. It is also possible to identify individual grains, most likely tetragonal ZrO_2.

CONCLUSION

The results of studies of densification, phase composition, microstructure and some properties of mullite-ZrO_2-ceramics with the addition of Si_3N_4, obtained by traditional sintering, SPS, in a microwave furnace and in a solar furnace are presented. It was found that almost 100% densification of a ceramic sample is achieved only with SPS. In ceramic sam-

ples sintered in a microwave furnace and by the conventional method, densification decreases, respectively, to less than 90% and 80%. Due to formation of defects in samples sintered in a solar furnace, the degree of densification of samples with the addition of Si_3N_4 sharply decreases from 90 to below 70% when 5% Si_3N_4 is introduced. Respectively, compressive strength correlates with densification: from 598 MPa in the samples obtained by SPS to 395 MPa and 98 for the samples sintered in a microwave furnace and by the conventional method, respectively. Elastic moduli of ceramic samples obtained by the conventional method and by SPS are relatively high at 140 and 180 GPa, respectively. After thermal shock cycles, the elastic modulus values of the conventionally sintered samples decrease and approach zero. In ceramic samples obtained by SPS with increasing number of thermal shock cycles, and especially in samples without the addition of Si_3N_4, the elastic modulus values do not decrease by more than about 30%, making it possible to classify these ceramic samples as heat-resistant.

The microstructure of ceramic samples sintered by the conventional method, by reactive spark plasma sintering, by microwave sintering, and by sintering in a solar furnace is characterized by the presence of characteristic closely packed prismatic or pseudo-prismatic mullite formations, especially in SPS samples. In ceramics sintered by the conventional method, and in ceramics sintered by other methods, voids (closed pores) are formed, in which secondary crystallization takes place. Sintering in a solar furnace at this stage of the research has not yielded positive results, since it is necessary to optimize the size of the initial samples and the sintering regime for this type of sintering.

The work was financed by the European Regional Development Fund within the project 1.1.1.1/16/A/077 "Mining and synthetic nano powders for obtaining porous ceramics and modification of ceramic materials" and within the project SFERA PROJECT 2017 "Mullite-zirconia refractory materials development by solar furnace sintering".

REFERENCES

1. M. Malki, C. M. Hoo, M. L. Mecartery, and H. Schneider, "Electrical conductivity of mullite ceramics," *J. Am. Ceram. Soc.*, **97**, 1923 – 1930 (2014).
2. N. Rendtorff, L. Garrido, and E. Aglietti, "Mullitezirconia-zirconcomposites: Properties and thermal shock resistance," *Ceram. Int.*, **35**(2), 779 – 786 (2008). https://doi.org/10.1016/j.ceramint.2008.02.0/.
3. K. Das, S. K. Das, B. Mukherjee, and G. Barnerjee, "Microstructural and mechanical properties of reaction sintered mullite-zirconia composites with magnesia as additive," *Interceram.*, No. 5, 304 – 616 (1998).
4. D. Pereira, G. R. S. Biasibetti, R. V. Camerini, and A. S. Pereira, "Sintering of mullite by different methods," *Materials and Manufacturing Processes*, **29**(4), 391 – 396 (2014). https://doi.org/10.1080/10426914.2013.864400.
5. Kuo Hsien-Nan, Chou Jyh-Horng, and Liu Tung-Kuan, "Microstructure and mechanical properties of microwave sintered ZrO_2 bioceramics with TiO_2 addition," *Applied Bionics and Biomechanics*, Vol. 2016, Article ID 2458685, 7 p. (2016) http://dx.doi.org/10.1155/2016/2458685.
6. S. Bodhak, S. Bose, and A. Bandyopadhyay, "Densification study and mechanical properties of microwave-sintered mullite and mullite-zirconia composites," *J. Am. Ceram. Soc.*, **94**(1), 32 – 41 (2011). doi: 10.1111/j.1551-2916.2010.04062.x.
7. P. M. Souto, M. A. Camerucci, A. G. T. Martinez, and R. H. G. A. Kiminami, "High-temperature diametral compression strength of microwave-sintered mullite," *J. Eur. Ceram. Soc.*, **31**, 2819 – 2826 (2011). doi:10.1016/j.jeurceramsoc.2011.07.034.
8. N. Zhilinska, I. Zalite, J. Rodriguez, et al., "Sintering of nanodisperse powders in a solar furnace," *Eur. Powder Met. Conf. 2003* (*EuroPM 2003*), Valencia, 423 – 428 (2003).
9. R. Roman, I. Canadas, J. Rodriguez, et al., "Solar sintering of alumina ceramics: microstructural development," *Solar Energy*, **82**, 893 – 902 (2008). doi: 10.1016/j.solener.2008.04.002.
10. G. Sedmale, M. Rundans, I. Sperberga, et al., "Ceramic of the mullite–ZrO_2/Y_2O_3–SiAlON system during spark plasma sintering," *Refract. Ind. Ceram.*, **57**(2), 146 – 150 (2016).